Geotechnical Aspects of Underground Construction in Soft Ground – Yoo, Park, Kim & Ban (Eds)

Advanced numerical modelling of multi-storey buildings response to tunnelling

D. Boldini, V. Fargnoli & C.G. Gragnano
University of Bologna, Bologna, Italy

A. Amorosi
Technical University of Bari, Bari, Italy

ABSTRACT: In this study the interaction between the ground and a reinforced-concrete building during tunnelling is investigated by a fully coupled three-dimensional approach using the Finite Element code PLAXIS 3D. The excavation of the Milan underground new line 5 by an earth pressure balance (EPB) machine in granular soils is taken as reference for tunnel characteristics and ground conditions. A number of ideal multi-storey reinforced-concrete buildings with appropriate stiffness and weight is examined, all of them being located in a symmetric position with respect to the tunnel. The analysis is also extended to highlight the stiffening contribution of the infill external panels of the structures, schematised as equivalent cross-bracings, on the transversal and longitudinal settlement profiles. The attention is also focused on the evolving response shown by the building columns, evaluated in terms of normal compression forces, during the excavation process.

1 INTRODUCTION

Several cities worldwide are currently involved in the construction of underground metro lines or high-speed railways to promote public transportation. A key aspect of these projects is represented by the interaction of excavation works with existing above- or underground structures located nearby (e.g. Amorosi et al., 2014). In some cases, as in several Italian cities, the tunnels are constructed under a very unique and fragile historical and monumental environment to be preserved from any possible induced damage (e.g. Rampello et al., 2012). This aim can be pursued through a very careful and detailed design strategy and by applying the most advances construction techniques associated to an extensive monitoring system.

The use of numerical methods is nowadays common to predict tunnelling-induced displacement field, which is generally modified by the presence of interacting structures. The success of such methods in practical applications strongly depends on many different variables, including the adopted soil constitutive hypotheses (e.g. Gonzales et al., 2012), the schematisation of the complex construction sequence (e.g. Kasper & Meschke, 2004) and the representation of the essential features of the structural response (e.g. Son & Cording, 2011).

In this paper an advanced numerical approach, based on a fully 3D solution scheme, is presented with the aim to investigate soil-structure interaction problems during tunnelling. The soil is modelled assuming an advanced constitutive law, the Hardening Soil model with small-strain stiffness (HSsmall, Benz, 2006), available in the material model library of the Finite Element (FE) code adopted in this study (PLAXIS 3D).

Tunnel characteristics as well as ground conditions are selected with reference to the excavation of the new Milan metro-line 5 (Fargnoli et al., 2013) between the stations of *Lotto* and *Portello*. The subsidence induced by the excavation of the first tunnel (i.e. right tunnel) of the line by an earth pressure balance (EPB) machine is first analysed under free-field conditions and then extended to include ideal structural models of 2, 4 and 8-storey reinforced-concrete framed buildings with different characteristics of stiffness and weight. The study is also intended to explore the role of the infill external panels of the structures, schematised by means of equivalent cross-bracings, on the overall settlement pattern.

2 THE CASE STUDY: TUNNEL EXCAVATION AND GROUND CONDITIONS

The portion of the new Milan metro-line 5 considered in this study extends underground the city for a length of about 600 m between *Lotto* and *Portello* stations.

The twin tunnels of the line were excavated in coarse-grained material partially under the water table. The distance between the two tunnel axes and their mean depth, z_0, are both equal to 15 m. In order to minimise ground movements in these highly urbanised

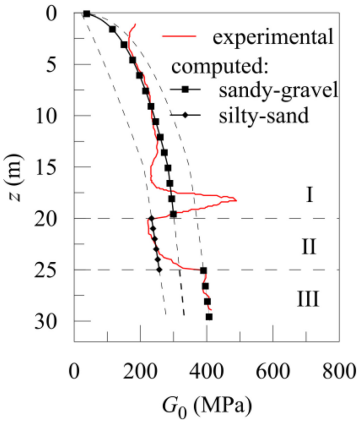

Figure 1. Experimental and computed profiles of small strain shear modulus with depth.

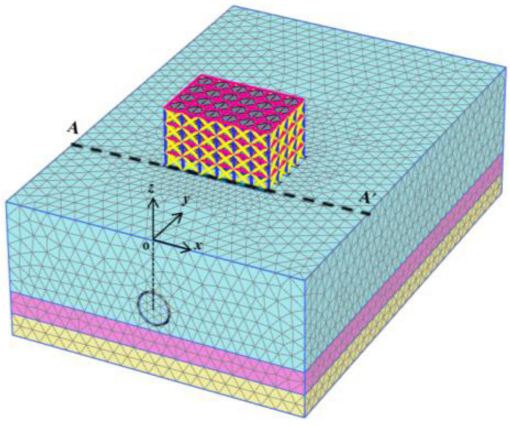

Figure 2. Sketch of the mesh.

areas, an EPB machine was selected, having a diameter, D, of about 6.7 m and a 10 m long shield. The tunnel lining consists of pre-cast concrete rings with a length of 1.4 m and a thickness of 30 cm. The outer and inner diameters of the lining ring are equal to 6.40 m and 5.80 m, respectively.

The soil profile at the location under investigation is constituted by sandy-gravel soil, the main component of the deposit, at depths between 0–20 m and 25–30 m and by a layer of sandy-silt, about 5 m thick, between 20–25 m. The total unit weights for saturated conditions, γ, for these materials are equal to 20 kN/m^3 and 17.5 kN/m^3, respectively.

Results of SPT tests conducted in the sandy-gravel deposit were elaborated following Skempton (1986), leading to a relative density in the range of 60–80% and strength parameters equal to $c' = 0$ kPa and $\phi' = 33°$. In absence of specific tests conducted on the sandy-silt material, typical strength properties are assumed (i.e. $c' = 5$ kPa and $\phi' = 26°$). The mean depth of the hydrostatic water table in the examined portion of the route is about 15 m from the ground level.

No geophysical investigations were specifically undertaken for this project; the one nearest to the reference segment of the route is a down-hole test performed at a nearby construction site in very similar geotechnical conditions: this test results in the small strain shear modulus (G_0) profile shown in Figure 1.

3 FINITE ELEMENT MODEL

Different numerical models were set up to simulate the tunnel excavation under free-field conditions and in presence of three ideal 2, 4 and 8-storey reinforced-concrete framed structures. All the buildings have a dimension of 24 m × 16 m in plan, an inter-storey height of 3.2 m and bays 4 m long in both x and y directions. They are founded on 5 strip footings (1.2 m × 1 m × 25.2 m) warped along the x-axis and are composed by beams and columns, both with a section of 30 cm × 30 cm, and of floor slabs (22 cm thick). The presence of infill panels, 40 cm thick and uniformly distributed in the external frames, is taken into account in a simplified way, as discussed in section 3.3.

All the numerical simulations were performed using the commercial Finite Element code PLAXIS 3D. The size of the mesh (68 m × 10 m 30 m) employed in the present study (Fig. 2) was found to minimise the influence of boundary conditions on the computed results.

Nodes at the bottom of the mesh are fixed in both vertical and horizontal directions, while the vertical boundaries are only fixed in the horizontal direction. The soil domain, as well as the foundation elements, are discretised by 10-node tetrahedral elements, while 2-node elastic anchor elements, 3-node line beam elements and 6-node triangular plate elements are used to model the structures and some components of the tunnel (i.e. the shield and the lining).

According to the *in situ* stratigraphy, the soil profile is constituted by two layers of sandy-gravel (between 0–20 m and 25–30 m) and a layer of sandy-silt (between 20–25 m); the imposed water table is 15 m below the ground surface.

The tunnel ($D = 6.7$ m) is located at a depth of $z_0 = 15$ m. It underpasses the surface structures without any eccentricity (Fig. 2). The foundation level is situated 1 m below the ground surface.

An interface with a strength controlled by the soil parameters is introduced in the model solely between the tunnel shield and the soil, while no interfaces are defined at the soil-lining and soil-building contacts.

All the numerical analyses are performed in terms of effective stresses, assuming for the soils drained conditions.

3.1 *Soil constitutive model*

The mechanical behaviour of sandy-gravel and sandy-silt soils is described by the advanced Hardening Soil model with small-strain stiffness (HSsmall). Such

constitutive model is capable of taking into account the very high soil stiffness observed at very low strain levels, its variation with strain level and the early accumulation of plastic deformations (Benz, 2006).

A summary of all model parameters and corresponding values is provided in Table 1.

The total unit weight (γ) and the strength parameters (c' and ϕ') of the soil were determined as previously discussed in section 2. For sake of simplicity, it is assumed the same γ value for the soils above and below the water table.

The variation of the small strain stiffness with depth is obtained by calibrating the parameters G_0^{ref} and m against the down hole experimental results, as shown in Figure 1.

The dependency of the shear stiffness with the strain level is introduced by referring to the experimental curves G/G_0-γ proposed by Vucetic and Dobry (1991) for granular soils (index of plasticity $I_P = 0$) and for material with a low plasticity (index of plasticity $I_P = 15\%$), respectively for the layers of sandy-gravel and sandy-silt.

The reference value of the Young's modulus at small strains, $E_0^{'ref}$, is related to G_0^{ref} by the Poisson's ratio for unloading/reloading, υ_{ur}. Starting from $E_0^{'ref}$ values and according to the stiffness reduction curves, the reference unloading/reloading stiffness at engineering strains ($\gamma = 0.1\%$), $E_{ur}^{'ref}$, is assumed to be $0.24E_0^{'ref}$ for granular soil and $0.42E_0^{'ref}$ for sandy-silt. The other stiffness parameters, $E_{50}^{'ref}$ and $E_{oed}^{'ref}$, are assumed as being three times lower than $E_{ur}^{'ref}$.

For the sake of simplicity the dilatancy angle, ψ, is assumed to be zero for both materials. Finally, for all soils the overconsolidation ratio is fictitiously assumed very large with the only scope of excluding yielding on the cap surface and to reproduce numerically the high value of the yield stress in compression.

Table 1. HS small model parameters and values.

	Values		
Parameters	I layer	II layer	III layer
Failure parameters:			
c' (kPa)	0	5	10
ϕ'(°)	33	26	33
ψ (°)	0	0	0
Stiffness parameters:			
m (–)	0.4	0.85	0.4
$E_{50}^{'ref}$ (kPa)	52000	54250	63856
$E_{oed}^{'ref}$ (kPa)	52000	54250	63856
$E_{ur}^{'ref}$ (kPa)	156000	162750	191568
υ_{ur} (–)	0.3	0.25	0.3
G_0^{ref} (kPa)	250000	155000	307000
$\gamma_{0.7}$(–)	0.0001	0.0002	0.0001
Other parameters:			
p^{ref} (kPa)	100	100	100
K_0^{nc} (–)	0.455	0.562	0.455
R_f (–)	0.9	0.9	0.9
$\sigma_{tension}$	0	0	0
$c_{increment}$ (kPa/m)	0	0	0

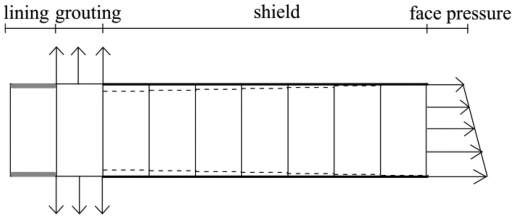

Figure 3. Schematisation of EPB tunnelling.

3.2 *EPB tunnelling numerical schematisation*

In all the numerical analyses the following sequence is adopted:

- initialisation of the stress field in the soil;
- activation of the surface building in a single step (only in the interaction analyses);
- tunnel excavation in several steps (in the first step the displacement field due to the gravity is reset to zero).

The simplified numerical procedure adopted to model the tunnel construction is illustrated in Figure 3. The excavation is simulated for 70 m by a step-by-step procedure consisting in 43 advancements having the length of one concrete lining ring (1.4 m). The advancement consists in the removing of one slice of soil inside the tunnel, assuming for these elements dry conditions. At the new tunnel face a pressure is applied, corresponding to the estimated total horizontal stress at rest $\sigma_{h0}(z)$ and ranging from 106 kPa at the tunnel crown to 185 kPa at the invert.

At any stage, the tunnel cavity is wholly lined by the shield, which extends for a total length of 9.8 m (i.e. 7 slices) or by the permanent lining, which is installed at the back of the shield. This latter and the lining are modelled using plate structural elements with an isotropic linear elastic behaviour having the following properties: thickness equal to 0.03 m, unit weight of 75 kN/m^3, Poisson's ratio equal to 0.25 and Young's modulus of 210 GPa for the shield; thickness equal to 0.3 m, unit weight of 25 kN/m^3, Poisson's ratio equal to 0.15 and Young's modulus of 35 GPa for the lining.

In the intermediate zone between the shield tail and the permanent lining, a region of 1.4 m of unlined soil is supported by a uniform pressure of 172 kPa, this latter being the mean value of the grouting pressure recorded during the excavation stage along this segment of the route (Fargnoli et al., 2013). In order to control the subsidence volume at the ground surface, a fictitious contraction, compatible with the available gap of the reference EPB machine, is applied along the shield. Such contraction, starting from the second slice of the shield, is characterised by a constant increment along each slice, so as to reproduce in a simplified way the shield conical geometry.

3.3 *Numerical modelling of the buildings*

2, 4 and 8-storey reinforced-concrete framed buildings were introduced in the FE model schematising their main structural components as follows (Gragnano et al., 2014):

- beams and columns are modelled by beam elements;
- plate elements with isotropic behaviour are used for the floor slabs;
- the foundations are represented by volume elements constituted by non-porous material.

A linear-elastic constitutive law is adopted for all the structural components, whose parameters are selected consistently with the reinforced-concrete material properties: unit weight $\gamma = 24\ \text{kN/m}^3$, Young's modulus $E_c = 25$ GPa, Poisson's ratio $\nu = 0.2$.

The external infill panels are schematised by means of equivalent cross bracings having a width, b_w equal to 53 cm, defined according to Mainstone (1971). They are modelled as weightless one-dimensional node-to-node anchor elements reacting only to axial stresses and characterised by an axial stiffness equal to $K = E_w * b_w * t_w$, where the Young's modulus of the infill panel $E_w = 3$ GPa and the panel thickness $t_w = 40$ cm.

4 NUMERICAL RESULTS

A preliminary free-field numerical analysis (FF) was performed to calibrate the contraction to be applied at the tunnel profile to reproduce a volume loss equal to about 0.3%, corresponding to that observed on average at the Milan construction site. The computed transversal (Fig. 4*a*) and longitudinal (Fig. 4*b*) surface profiles are in fair agreement with the Gaussian curve (Peck, 1969) and the cumulative Gaussian curve (Mair and Taylor, 1997), this latter translated in order to take into account the effect of the support pressure acting at the tunnel face. The overall satisfactory comparison between the steady-state computed profiles and the empirical ones, obtained with $K = 0.45$ and assuming $i_x = i_y = 6.75$ m, confirms the ability of the numerical model to reproduce realistic results.

This preliminary FF analysis was followed by the interaction ones, all carried out imposing the same excavation sequence and amount of contraction defined above, but this time in presence of different surface structures. Reference analyses (STR) were performed considering 2, 4 and 8-storey buildings, characterised by their appropriate weight and stiffness, this latter also enhanced by the inclusion in the structural models of the external infill panels, by means of specific cross-bracings.

The transversal and longitudinal settlement profiles computed by the STR analyses at the foundation level ($z = -1$ m) are compared in Figure 5(*a*) and (*b*), where the free-field numerical curves (FF) are also shown. In particular, the proposed transversal troughs are those

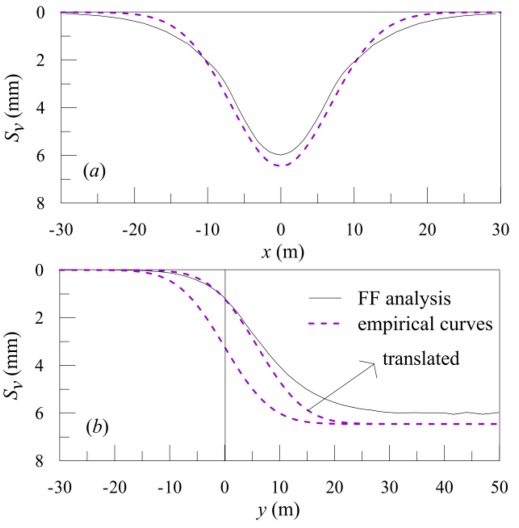

Figure 4. Comparison between numerical and empirical free-field subsidence profiles in transversal (*a*) and longitudinal (*b*) directions for $V_L = 0.31\%$.

resulting along section A-A′ of the model (Fig. 3), i.e. in correspondence of the main building façade.

In general, it is possible to observe that the taller the structure, the larger the maximum settlement and the extension of the curve as compared to the free-field one, and the greater the computed V_L. This latter feature should also be related to the dependency of the adopted constitutive model on the effective stress state, leading to the non-negligible role of the weight of the structure.

Figure 5(*a*) points out that the profiles of the interaction analyses are characterised by lower differential settlements as compared to the free-field curve, while they exhibit larger vertical displacements at the building edges, which indicate their embedment into the soil. Such a result, more evident for the 8-storey structure, is consistent with what observed by Farrell and Mair (2011) in their centrifuge experiments.

Figure 5(*b*) clearly highlights the stiffer response observed in correspondence of the foundation elements, whose position is reported by dashed lines. It also shows the non-uniform subsidence profiles under the building, to be related to the effect of the weight distribution.

The contribution of the cross-bracings and the influence of the weight of the structure were investigated in the analyses denoted STR_{wcb} and STR_{w}, respectively. In particular, in the first set of analyses the buildings were modelled without cross-bracings, while in the second the structures were reduced to their corresponding non-uniform stress distributions acting at the strip footings levels, 1 m below the ground surface. The numerical outcomes are compared in Figures 6(*a*) and (*b*) with reference to the 8-storey case.

As displayed in Figure 6(*a*), all the settlement troughs approximately intersect at i_x and overlap for

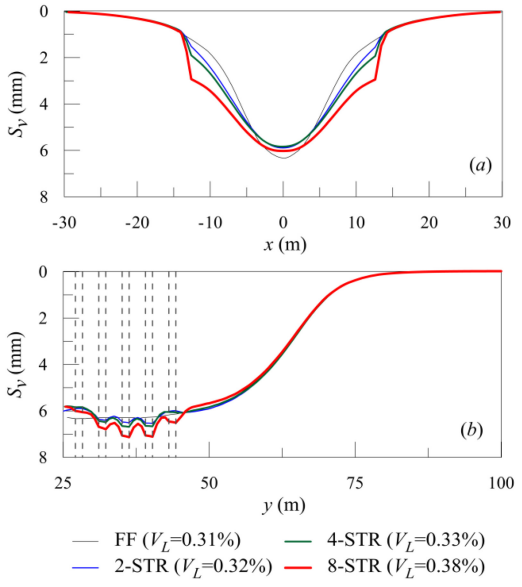

Figure 5. Computed transversal (*a*) and longitudinal (*b*) settlement profiles of FF and STR analyses.

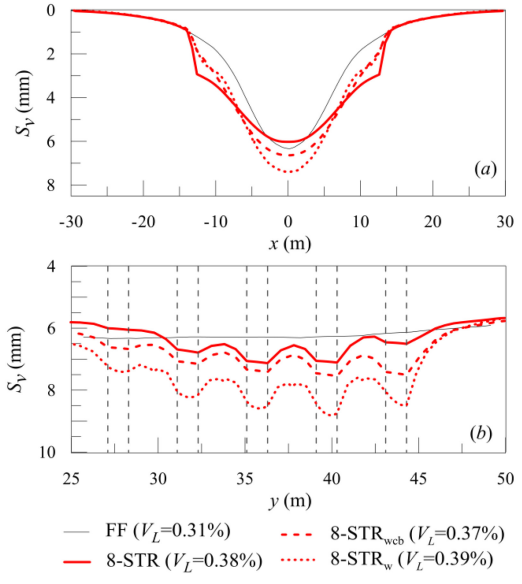

Figure 6. Computed transversal (*a*) and longitudinal (*b*) settlement profiles.

x values located outside the building area. In particular, Figure 6 highlights the stiffening role of the cross-bracings, which leads to a modification of the settlement pattern along both directions.

In Figure 6(*b*) it appears that such an effect is more evident in correspondence of the less loaded foundation elements (i.e. the external strip footings).

As expected, larger maximum and differential settlements are obtained by neglecting the overall stiffness of the structure, i.e. only considering its own

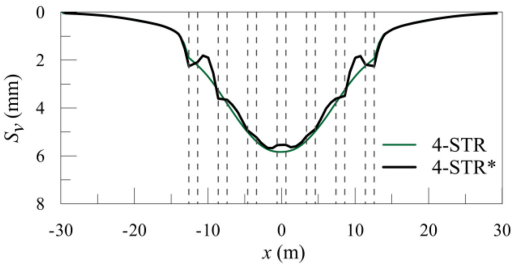

Figure 7. 4-storey building: comparison between STR* and STR subsidence profiles.

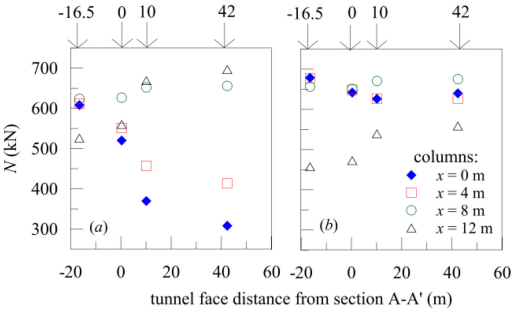

Figure 8. STR (*a*) and STR$_{wcb}$ (*b*) analyses: N values acting in the columns at the excavation progress.

weight in the numerical analyses, despite the small variation in terms of volume loss.

The role of the foundation warping direction was explored by analysis 4-STR*, where the foundation beams of the 4-storey building were oriented along the y-axis, to be compared to the corresponding 4-STR analysis in which the warping direction was along the x-axis. Such comparison is shown in Figure 7, where the foundation elements are reported by dashed lines. The figure highlights that, as expected, the 4-STR* transversal settlement profile is more discontinuous than the reference one, while characterised by rather similar values of vertical displacements computed in correspondence of the strip footings.

The analysis of the results was also extended to compare the evolving response shown during the tunnelling process by the columns composing the main façade of the structure. Due to symmetry, the sole response of the columns located on the right side of the building was examined. For sake of brevity, in the following the discussion is limited to the 8-storey building. In particular, the normal compression forces (N) acting at the columns base ($z = 0$ m and $x = 0$ m, $x = 4$ m, $x = 8$ m and $x = 12$ m) are shown in Figure 8(*a*) and (*b*) for different tunnel face positions (indicated by arrows in the figure).

It is possible to observe (Fig. 8*a*) that when the front is far from to the examined section (e.g. 16.5 m before the section), the columns at $x = 0$ m, $x = 4$ m and $x = 8$ m are characterised by the same N value.

This latter coincides with that due to the building self-weight and it is greater than the one acting in the outer column ($x = 12$ m).

During tunnelling, the normal force decreases in the inner columns (i.e. those at $x = 0$ m and $x = 4$ m), while in the outer ones, affected by lower settlements, it exhibits an opposite trend. At the end of the excavation sequence, N reaches its maximum value in the column at $x = 12$ m, which experiences the lowest vertical displacement. This is due to the process of forces redistribution within the structure, which is enhanced by the presence of the cross bracings.

The absence of the cross-bracings in the numerical model (STR_{wcb} analysis) inhibits the load transfer within the structure: in fact in this case, illustrated in Figure 8(*b*), during tunnelling N values in the inner columns are rather constant, while the normal stress evolution in the outer one is similar to that of Figure 8(*a*), but for lower values of normal compression forces.

5 CONCLUSIONS

This paper presents the results of a Finite Element study, conducted by the numerical code PLAXIS 3D, devoted to assess the response of 2, 4 and 8-storey ideal reinforced-concrete framed buildings, characterised by real features in terms of weight and stiffness, affected by tunnelling-induced settlements. Tunnel details as well as soil conditions refer to the case-history of the new Milan underground line 5, excavated adopting EPB machines in coarse-grained soils. The study was carried out assuming for the soil the constitutive law named Hardening Soil model with small-strain stiffness (HSsmall), calibrated against in situ tests, and simulating the tunnel construction process by a detailed step-by step procedure.

A preliminary free-field analysis, followed by the interaction ones, was performed to reproduce a volume loss value equal to $V_L = 0.31\%$, as observed on average at the Milan construction site.

The numerical outcomes highlight that, in general, the presence of a surface structure substantially modify the free-field transversal and longitudinal subsidence profiles. More specifically, the taller and heavier is the structure, the larger are the maximum settlements and the lower the differential ones. Greater vertical displacements are obtained by neglecting the overall stiffness of the structure or the stiffening contribution provided by its external infill panels, although modelled in a simplified way (i.e. as equivalent cross bracings).

An attempt to explore the evolving response of the columns composing the main façade of the 8-storey building during tunnelling is presented in the last part of the paper. It was pointed out that the process of forces redistribution within the structure is enhanced by the presence of the cross bracings.

ACKNOWLEDGEMENTS

Special thanks to Dr. Francesco Tucci for his suggestions offered in the analysis of structural response.

REFERENCES

Amorosi, A., Boldini, D., de Felice, G., Malena, M. & Sebastianelli, M. (2014). Tunnelling-induced deformation and damage on historical masonry structures. *Géotechnique* 64(2), 118–130.

Benz, T. (2006). Small-strain stiffness of soils and its numerical consequences. *Ph.D. thesis*, Universität Stuttgart.

Fargnoli, V., Boldini, D. & Amorosi, A. 2013. TBM tunnelling-induced settlements in coarse grained soils: the case of the new Milan underground line 5. *Tunnelling and Underground Space Technology*: 38, 336–347.

Farrell, R.P. & Mair, R.J. (2011). Centrifuge modelling of the response of buildings to tunnelling. *Proceedings of 7th International Symposium on Geotechnical Aspects of Underground Construction in Soft Ground, Rome*, pp. 343–351.

Gonzalez, N. A., Rouainia, M., Arroyo, M. & Gens, A. (2012). Analysis of tunnel excavation in London Clay incorporating soil structure. *Géotechnique* 62, No. 12, 1095–1109.

Gragnano, C.G., Fargnoli, V., Boldini, D. & Amorosi, A. 2014. Comparison of structural elements response in PLAXIS 3D and SAP2000. *Plaxis Bulletin*, Issue 35/Spring 2014: 6–11.

Kasper, T. & Meschke, T. (2004). A 3D finite element simulation model for TBM tunnelling in soft ground. *Int. J. Numer. Analyt. Methods Geomech.* 28 (14), 1441–1460.

Mainstone, R.J. 1971. On the stiffnesses and strengths of infilles frames. *Proc. Inst. Civil. Engineers, iv 7360s*: 59–70.

Mair, R.J., Taylor, R.N. (1997). Bored Tunnelling in the urban environment. State-of-art-report and theme lecture. *Proceedings of the 14th international conference on soil mechanics and foundation engineering, Hamburg*, Balkema, vol. 4, pp. 2353–2385.

Peck, R.B. (1969). Deep excavations and tunnelling in soft ground. *Proceedings of the 7th international conference on soil mechanics and foundation engineering*, Mexico City, pp. 225–290.

Rampello, S., Callisto, L., Viggiani, G. & Soccodato, F. (2012). Evaluating the effects of tunnelling on historical buildings: the example of a new subway in Rome. *Geomech. Tunnelling* 5 (3), 275–299.

Skempton, A.V. 1986. Standard penetration test procedures. *Géotechnique* 36 (3), 425–557.

Son, M. & Cording, E.J. (2011). Responses of buildings with different structural types to excavation-induced ground settlements. *J. Geotech. Geoenviron. Engng*. 137 (4).

Vucetic, M. & Dobry, D. 1991. Effect of Soil Plasticity on Cyclic Response. *Journal of Geotechnical Engineering*: 117, 89–107.